Azimuthal distributions and collective motion in intermediate energy heavy-ion collisions

W.K. Wilson,[1,*] W. Bauer,[1] D Cebra,[1,†] M. Cronqvist,[1,‡] D. Krofcheck,[1,‡] R. Lacey,[1,§] T. Li,[1] A. Nadasen,[2] E. Norbeck,[3] T. Reposeur,[1] A. Vander Molen,[1] C.A. Ogilvie,[1,‖] G.D. Westfall,[1] J.S. Winfield,[1] and J. Yee[1]

[1] *National Superconducting Cyclotron Laboratory and Department of Physics and Astronomy, Michigan State University, East Lansing, Michigan 48824*

[2] *Department of Natural Sciences, University of Michigan, Dearborn, Michigan 48128*

[3] *Department of Physics, Iowa State University, Des Moines, Iowa 99999*

(Received 26 January 1995)

The azimuthal distributions of light particles (Z=1,2) with respect to the entrance channel reaction plane are investigated for Ar+V collisions in order to characterize the modes of collective motion in intermediate energy heavy-ion reactions. At a beam energy of 35 MeV/nucleon, light charged particles are found to exhibit an enhanced emission in the reaction plane which increases with the mass of the detected particle. As the beam energy is increased to 100 MeV/nucleon, the anisotropy nearly vanishes, providing insight into the dynamics of these reactions in a transitional energy regime. The observed anisotropy exhibits signatures of two distinct modes of collective motion: attractive mean-field deflection and rotation of the fused system. A microscopic calculation based on mean-field mediated interactions plus nucleon-nucleon collisions reproduces both forms of collective motion and their associated azimuthal anisotropies. The calculation also suggests that the anisotropy due to mean field deflection is established during the initial stages of the collision.

PACS number(s): 25.70.Mn, 24.10.Cn

I. INTRODUCTION

At incident energies near the Fermi energy, the azimuthal distributions of light particles produced in heavy-ion collisions have been shown to exhibit strong peaks in the reaction plane [1]. In this paper we present the results of a study of azimuthal distributions of Z=1,2 particles produced in Ar+V collisions and detected by the Michigan State University (MSU) 4π Array. Some of the initial results of these experiments were presented in Ref. [2]. In this paper, we describe the experiments in greater detail and compare the results to theoretical expectations. The goal is to provide further insight into the nature of the reaction mechanisms in intermediate-energy collisions by investigating the relationship between azimuthal anisotropy and modes of collective motion. In contrast to relativistic collisions in which compression leads to a hydrodynamical side splash and squeeze out [3–5], collective motion in the intermediate energy range is dominated by the attractive component of the nuclear mean field [6–8].

We begin by examining the influence of two simple forms of collective motion, rotation and attractive flow (or mean field deflection), on the azimuthal distributions of emitted particles. A parametrization of the azimuthal anisotropy will be introduced in order to clearly distinguish between the contributions of the different modes of collective motion. Using this technique in the analysis of 35 MeV/nucleon Ar+V collisions, we show that signatures of both rotation and flow are present in our data. Next, we will explore the beam energy dependence of collective motion as $E_{\rm beam}$ is increased from 35 to 100 MeV/nucleon. We find increasing azimuthal isotropy with increasing beam energies, and this result is interpreted in terms of the decreasing role of the attractive component of the nuclear mean field. Finally, we compare our observations with a calculation using the Boltzmann-Uehling-Uhlenbeck (BUU) transport equation to further explore the relationship between the azimuthal anisotropies observed in the data and simple modes of collective motion in the collision.

*Present address: Physics Department, Wayne State University, Detroit, MI 48201.

†Present address: Physics Department, Universiyt of California, Davis, CA 95616.

‡Present address: Lawrence Berkeley Laboratory, Berkeley, CA 94720.

§Present address: Chemistry Department, State University of New York, Stony Brook, NY 11794

‖Present address: Physics Department, Massachusetts Institute of Technology, Cambridge, MA 02139.

II. EXPERIMENTAL DETAILS

A. Setup

Beams of ^{40}Ar at energies of 35, 45, 55, 65, 75, 85, and 100 MeV/nucleon were produced by the K-500 and K-1200 cyclotrons at the National Superconducting Cyclotron Laboratory. To obtain a nearly symmetric system, ^{51}V was chosen as the target. Charged fragments

were detected by the 170 phoswich telescopes of the MSU 4π Array Main Ball [9]. Isotopes of H were identified by their mass, while heavier fragments were identified by their charge. The addition of 45 phoswich telescopes arranged in a Forward Array brought the total angular coverage to 85% of 4π sr. The Forward Array gains were set to accept fragments with charges up to Z=8 for the 35 MeV/nucleon data. Angular, energy, and charge acceptances for the E/A=35 MeV/nucleon data are detailed in Ref. [10]. For the E/A=45 – 85 MeV/nucleon data, the charge acceptance in the Forward Array was extended up to Z=18 but mass resolution for H isotopes in these detectors was not obtained.

B. Analysis techniques

We characterized the impact parameter of the events by their mid rapidity charge, defined as the sum of charges which have rapidities from 75% of the target rapidity to 75% of the projectile rapidity in the center of mass (c.m.) frame [11]. The most peripheral events were discarded because of uncertainties in reaction plane determination for very low multiplicity events; the rest of the events were included in the analysis.

The reaction plane was determined on an event-by-event basis using azimuthal correlations. This technique for finding the reaction plane is described in detail in Ref. [12] and briefly in Refs. [7] and [2]. In essence, the technique exploits the existence of enhanced emission in the reaction plane by choosing the plane that aligns best with the enhanced emission.

III. SIMULATION STUDIES

A. Effects of collective motion on azimuthal distributions

In order to characterize the collective motion which produces the observed enhancement of particle emission in the reaction plane, it is desirable to parametrize the azimuthal anisotropy in a manner which decouples different forms of collective motion. Two distinct modes of collective motion have been proposed to explain various attributes of collisions observed in this beam energy range: rotation and flow. Rotational collective motion of the compound system about an axis perpendicular to the reaction plane was suggested by Tsang *et al.* [1,13] in the interpretation of two-particle azimuthal correlations. Flow due to attractive deflection by the mean field was invoked by Ogilvie *et al.* [10] to explain the dependence of the average transverse momentum in the reaction plane on rapidity.

Preferential emission in the reaction plane is observed for both rotation and flow, but the rapidity dependence is different for the two mechanisms. Rotation should enhance particle emission in the reaction plane equally on both sides of the beam axis at all rapidities. Flow, on the other hand, leads to an enhancement on one side of the reaction plane for particles going forward and on the other side for particles going backwards in the c.m. frame of reference. The side of the reaction plane, as divided by the beam axis, that contains the forward-going component of the flow is called the "forward flow side" of the reaction plane [12]. The differences between the effects of rotation and flow on azimuthal distributions are illustrated in Figs. 1 and 2 with simulated events. The top histograms of the two figures are rapidity distributions divided into six regions as indicated by the numbers used as plotting symbols. Within each event, we will refer to the particle whose azimuthal angle of emission is being investigated as the "particle of interest" (POI). The histograms underneath show the azimuthal distribution of POI with respect to the reaction plane for six POI rapidity cuts. As a convention, the azimuthal angles are always measured from the forward flow side of the reaction plane when flow was present. The reaction plane was found for each event using the technique described in Ref. [12].

The effects of rotation were simulated in Fig. 1 by flattening a Gaussian momentum distribution into an oblate shape of width σ, where

$$\sigma_x = \sigma_z > \sigma_y, \tag{1}$$

where the z axis is the beam axis, $\hat{x}$ is in the reaction plane, and $\hat{y}$ is normal to the surface of the plane and coincides with the direction of the angular momentum vector of the compound system. Consequently, in Fig. 1 the azimuthal distributions with respect to the found reaction plane peak equally at 0° and 180° at all rapidities. Note that although this is not a complete simulation of particle emission from a rotating source, it does exhibit most of the behavior of such a simulation. For example, this simulation produces azimuthal distributions which are invariant under rotations around the $\hat{y}$ (angular momentum vector) axis, and the in-plane enhancement increases with the energy of the emitted particle. These are the two most important properties of the equation

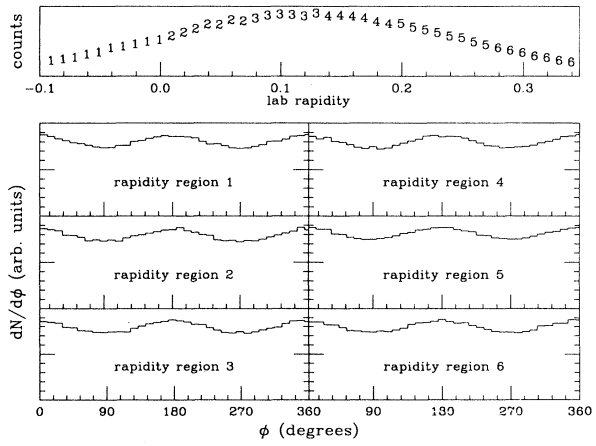

FIG. 1. Azimuthal distributions with respect to the reaction plane for an oblate momentum distribution simulating emission from a rotating source. The top histogram shows the positions of the six rapidity regions.

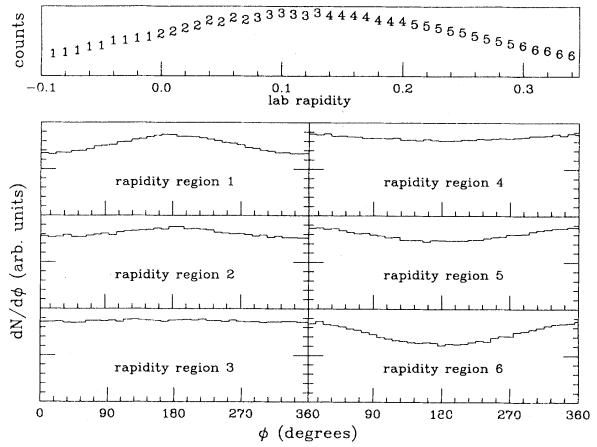

FIG. 2. Azimuthal distributions with respect to the reaction plane for a simulated source with transverse momentum flow.

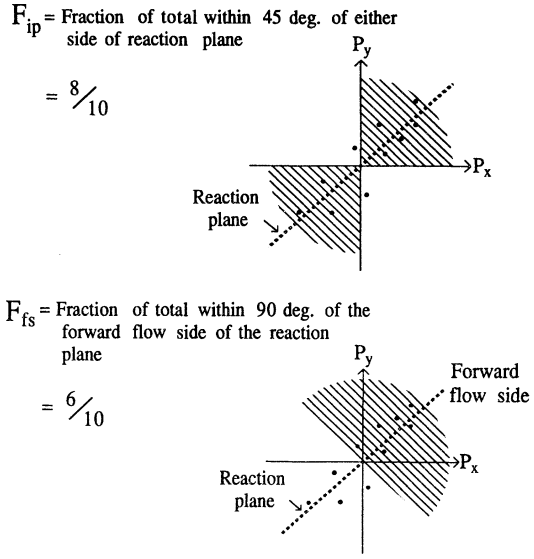

FIG. 3. Geometrical definition of the anisotropy parameters $F_{\rm ip}$ and $F_{\rm fs}$ projected onto the p_x–p_y plane.

for particle emission from a rotating sphere, derived in Ref. [14] by Chitwood *et al.*

In order to simulate flow in Fig. 2, the Gaussian momentum distribution was first stretched along the beam axis into a prolate shape, and then rotated slightly around the y axis (perpendicular to the reaction plane). Because the azimuthal angle of the POI is measured from the forward flow side of the reaction plane, the azimuthal distributions of Fig. 2 peak at around 0° at high rapidities, i.e., for POI going forward in the c.m. frame of reference. At mid rapidity the distribution is isotropic, while at the low rapidities the peaks reappear 180° away from the forward flow side. We exploited these differences between the azimuthal distributions generated by rotation and flow to create anisotropy parameters.

B. Parametrization of azimuthal distributions

The data can be conveniently characterized by two parameters, each chosen to be sensitive to only one form of motion. The rotation-sensitive parameter is $F_{\rm ip}$, the fraction of particles of interest found in the reaction plane. The flow-sensitive parameter is $F_{\rm fs}$, the fraction on the forward flow side of the reaction plane. The fractions are calculated by integrating over the azimuthal distributions:

$$F_{\rm ip} = \frac{\int_{-45^\circ}^{45^\circ} \frac{dn}{d\phi} d\phi + \int_{135^\circ}^{225^\circ} \frac{dn}{d\phi} d\phi}{\int_{0^\circ}^{360^\circ} \frac{dn}{d\phi} d\phi} \tag{2}$$

and

$$F_{\rm fs} = \frac{\int_{-90^\circ}^{90^\circ} \frac{dn}{d\phi} d\phi}{\int_{0^\circ}^{360^\circ} \frac{dn}{d\phi} d\phi}. \tag{3}$$

$F_{\rm ip}$ is simply the fraction of particles with azimuthal angles within 45° of the reaction plane, and $F_{\rm fs}$ is the fraction of particles within 90° of the forward flow side. The fractions are defined geometrically in Fig. 3. Quantitative relationships between the new parameters and other commonly employed parametrizations of azimuthal distributions are presented in the Appendix.

The rapidity dependence of the parameters clearly shows which forms of collective motion are present. The effects of rotation and flow on these parameters are displayed in the upper panels of Fig. 4 for simulated events.

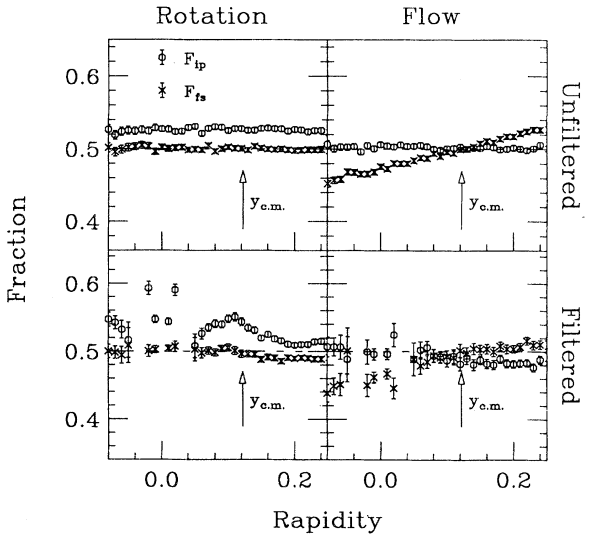

FIG. 4. Anisotropy fractions for a oblate momentum distribution simulating rotation (left panels) and a prolate distribution with transverse momentum flow (right panels). The simulations are shown before (top panels) and after (bottom panels) being passed through a software representation of the acceptance of the 4π Array. The dashed line represents the fractional value expected if the azimuthal distributions are isotropic.

The fraction of particles in the reaction plane, $F_{\rm ip}(y)$, deviates from isotropy [$F_{\rm ip}(y) = \frac{1}{2}$] only for the rotating source. The rotating source exhibits an $F_{\rm fs}(y) = 0.5$ at all rapidities because the in-plane enhancement occurs simultaneously on both sides of the reaction plane. Flow produces a non zero slope in $F_{\rm fs}(y)$ since particles are deflected towards the forward flow side of the reaction plane at high rapidities and towards the opposite side at low rapidities. On the other hand, since flow simply transfers particles from one side of the reaction plane to the other, it leaves the in-plane fraction $F_{\rm ip}(y)$ unchanged. Thus, an $F_{\rm ip}(y) > \frac{1}{2}$ is a signature of a momentum distribution similar to that expected due to particle emission from a rotating source, while a slope in $F_{\rm fs}(y)$ as a function of rapidity indicates the presence of collective flow in the reaction plane. These parameters are specific in the sense that $F_{\rm ip}(y)$ is sensitive only to rotation and $F_{\rm fs}(y)$ is sensitive only to flow. Note that the usual observable for measuring flow, the average transverse momentum in the reaction plane as a function of rapidity, is also insensitive to rotational collective motion.

C. Influence of detector acceptance

In order to isolate physical effects using experimentally observed anisotropy fractions, it is important to consider the influence of detector acceptance on the parameters. The simulated data shown in the upper panels of Fig. 4 were not filtered through the detector acceptance. Turning on the filter[1] produces the results shown in the lower panels of Fig. 4. (Points with very low statistics resulting in error bars larger than ± 0.04 are suppressed in these and all the forthcoming plots involving the anisotropy fractions in order to produce clearer plots. Data points with such very large error bars only occur at the extreme limits of the rapidity distribution.) Three significant effects emerge when the filtered simulations are compared to the unfiltered simulations.

The first effect is a discontinuity around $y_{\rm lab} = 0$ due to the finite polar angle granularity of the Main Ball. In the filtered events, each particle is assigned an angle which corresponds to the center of a telescope. There are no telescopes centered at 90° ($y_{\rm lab} = 0$), and data from telescopes on either side (87° and 93°) fall into several neighboring rapidity bins. The two bins closest to 90° contain only the lower-energy particles from these telescopes, while the next nearest set of bins contains the higher-energy particles from the same telescopes. Since higher-energy particles can only result when the thermal velocity adds constructively with the collective velocity, higher energy particles exhibit a stronger apparent collective motion. Therefore, it is the energy difference between particles found in the four bins around $y_{\rm lab} = 0$ that causes the discontinuity.

This discontinuity is suppressed in the other rapidity regions since the polar angles of the detectors overlap so as to contribute a wider range of particle energies to each rapidity bin. Smearing the assigned angles of detected particles over the faces of the telescopes rather than concentrating them at the centers will minimize the discontinuity.

The second effect of detector acceptance is a drop in $F_{\rm ip}(y)$ as the rapidity increases from 0.1 to 0.2 in the laboratory frame. Note that particles "see" a lower transverse momentum threshold as the rapidity increases over this region, as shown in Fig. 5. Therefore the drop occurs because lower thresholds decrease the observed anisotropy, again due to the addition of collective and thermal velocities as discussed previously. This drop can be eliminated by equalizing the transverse momentum cuts as a function of rapidity by excluding a cylindrically shaped region around the p_z axis (beam direction) in momentum space. The radius of the cylinder should be chosen to equal the maximum $p^{\perp}$ cut imposed by the detector acceptance.

The final influence of detector acceptance on the anisotropy parameters is due to multiple-hit exclusion, which is discussed in detail in Ref. [12]. Multiple-hit exclusion acts to effectively "repulse" the particle of interest from the reaction plane, creating a dip in the azimuthal distributions near 0° and 180°. Thus $F_{\rm ip}(y)$ is observed to decrease slightly for the filtered data. This effect is more pronounced at the higher rapidities since forward focusing of the reaction products makes the finite azimuthal granularity more important in that rapidity region. Therefore, in the lower right-hand panel of Fig. 4, where we would expect $F_{\rm ip}(y)$ to be $\frac{1}{2}$, we find that $F_{\rm ip}(y)$ drops slightly below the dashed isotropy line for the high-rapidity bins.

Another aspect of multiple-hit rejection is its effect on the $F_{\rm fs}(y)$ parameter at forward rapidities. Since the dip is deeper at 0° than at 180°, $F_{\rm fs}(y)$ is lowered from its un-

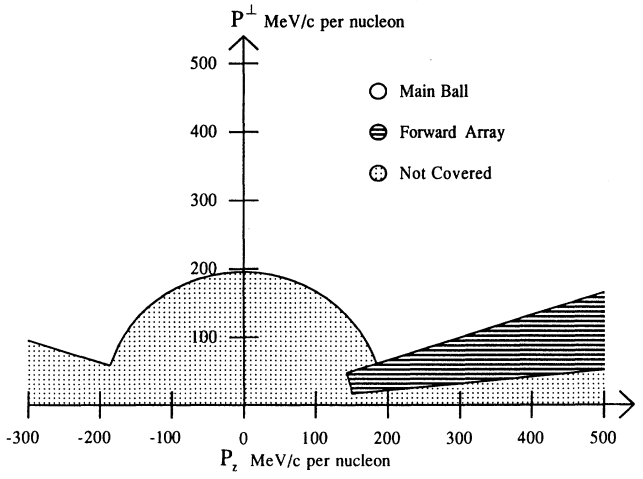

FIG. 5. Acceptance of 4π Main Ball + Forward Array system in momentum space in the laboratory frame of reference. The dotted region is not covered, and the region denoted by horizontal lines is covered by the Forward Array. The remaining regions are covered by the Main Ball.

[1]Copies of the 4π array filter code are available. Contact G.D. Westfall at WESTFALL@NSCL.NSCL.MSU.EDU for details.

filtered value, as can be seen in the lower left-hand panel of Fig. 4. The effect is stronger at 0° because, in the forward rapidity direction in the c.m. frame, most particles are emitted in the reaction plane on the forward flow side (0°), increasing the multiple-hit probability on that side relative to the opposite side of the reaction plane.

IV. EXPERIMENTAL RESULTS

A. 35 MeV/nucleon Ar+V

Measured anisotropy fractions for 35 MeV/nucleon Ar+V collisions are shown in Fig. 6 for both H and He particles. All of the features of the filtered rotation and flow simulations are reflected in the data, suggesting the presence of both modes of collective motion [2]. The presence of flow is revealed in Fig. 6 by the non zero slope in $F_{\rm fs}(y)$ at mid rapidity. The flow is stronger for He than for H, a trend that would be expected for collective velocity superimposed on random thermal motion. This is because thermal velocities decrease with increasing mass of the particles, leading to less random smearing of the collective velocity for He than for H.

The signature of preferential emission in the reaction plane, $F_{\rm ip}(y) > 0.5$, is particularly clear, suggesting the presence of rotational collective motion. Again, the effect is stronger for the heavier particles, as expected. In agreement with the filtered simulations, $F_{\rm ip}(y)$ varies with rapidity due to the variation in the detector thresholds. To provide a qualitative feeling for the magnitude of the observed anisotropies, the azimuthal distributions of H and He are shown in Figs. 7 and 8, respectively.

As stated earlier, the influence of changing $p^{\perp}$ thresholds can be eliminated by applying a common $p^{\perp}$ cut at all rapidities, and the effects due to polar angle granularity can be reduced by smearing the assigned angles over the solid angles subtended by the telescopes. When both of these techniques are applied to the 35 MeV/nucleon data, the resulting fractions are smoothly

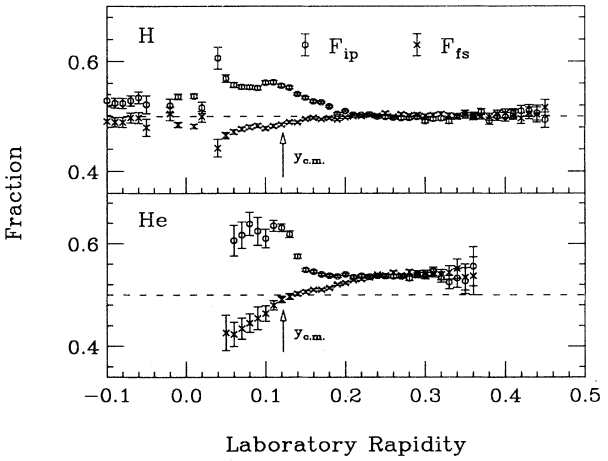

FIG. 6. Anisotropy fractions as function of rapidity for 35 MeV/nucleon Ar+V data.

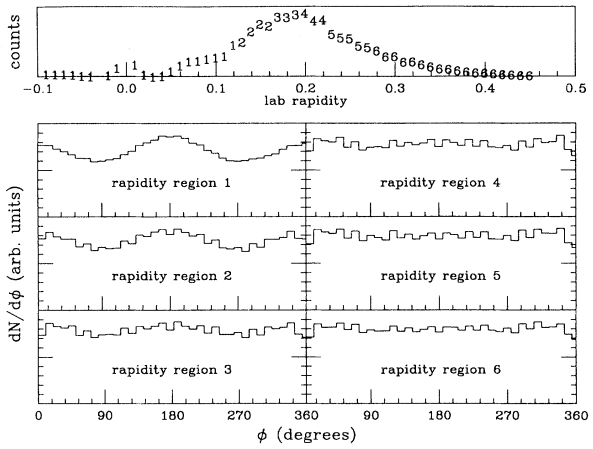

FIG. 7. Azimuthal distributions of hydrogen produced in 35 MeV/nucleon Ar+V collisions divided into six rapidity bins.

varying and more symmetric around the mid rapidity region (see Fig. 9). The deviation of $F_{\rm ip}(y)$ from isotropy closely resembles the $F_{\rm ip}(y)$ pattern expected for a rotating source, while the non zero slope of $F_{\rm fs}(y)$ in He reflects the presence of flow. There is a decrease in $F_{\rm ip}(y)$ at low rapidities compared to Fig. 6 caused by two separate mechanisms which we will discuss next.

The main cause of the drop in $F_{\rm ip}(y)$ in the H data can be determined from an inspection of the momentum dependence of $F_{\rm ip}(y)$ for various particle types. In Fig. 10 we see that the H ion with counts up to the highest transverse momentum is the proton, which also shows the weakest in-plane enhancement. Therefore, a higher $p^{\perp}$ cut tends to increase the relative number of protons in the H sample, accounting for the lower values of $F_{\rm ip}(y)$ seen in Fig. 9 as compared with the raw data. Also note that Fig. 10 demonstrates that the enhancement increases as mass increases from one to four nucleons as expected for collective motion. There is evidence in Fig. 10 for an increase in the in-plane enhancement up to a plateau value as the transverse momentum increases.

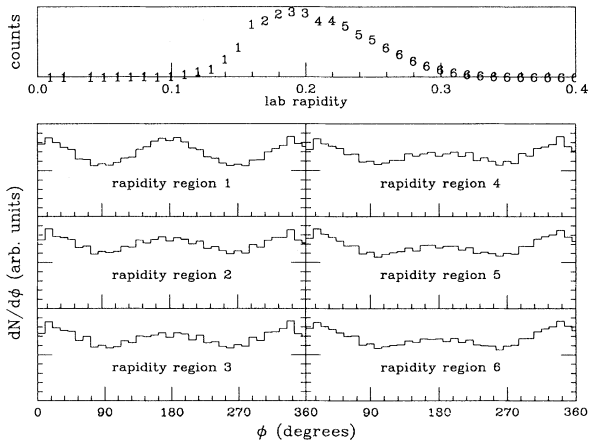

FIG. 8. Azimuthal distributions of helium produced in 35 MeV/nucleon Ar+V collisions divided into six rapidity bins.

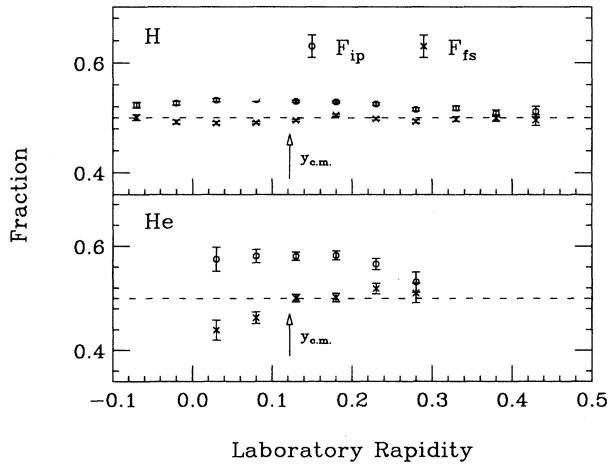

FIG. 9. Anisotropy fractions for 35 MeV/nucleon Ar+V data with $p^{\perp} \geq 210$ MeV/c per nucleon, smeared in angular assignments as described in the text.

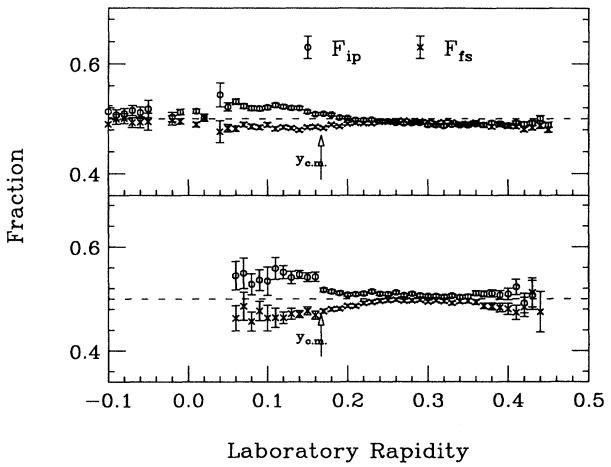

FIG. 11. Anisotropy fractions as function of rapidity for 65 MeV/nucleon Ar+V data.

There is also a slight loss in the accuracy of the reaction plane determination for the angle-smeared data compared to the raw data since the smearing used in the azimuthal direction was based on the maximum azimuthal width of the detectors.

B. Beam energy dependence

As the beam energy is increased to 100 MeV/nucleon, the collisions produce more azimuthally symmetric distributions of light particles. This can be seen from the anisotropy parameters shown in Figs. 11 and 12 for 65 and 100 MeV/nucleon Ar+V data, respectively. Note that in the higher-rapidity regions of Fig. 12, $F_{ip}(y)$ indicates a slight out-of-plane enhancement. However, this should not be interpreted as evidence for enhanced emission perpendicular to the reaction plane. Simulation studies of the detector acceptance show that the most probable cause is the increased forward focusing at the higher beam energies which magnifies the influence of multiple-hit exclusion.

The increasing isotropy of the events at higher beam energies is not simply due to the increase of the temperature of the composite system relative to the energy thresholds. The data in Fig. 13 show that there is no measurable enhancement in the reaction plane at any $p^{\perp}$ value for the 100 MeV/nucleon data at mid rapidity.

We can conclude that there must be a change in the mechanisms of collective motion as the beam energy is increased. For flow, this change has been demonstrated by plotting the forward-rapidity slope of the mean trans-

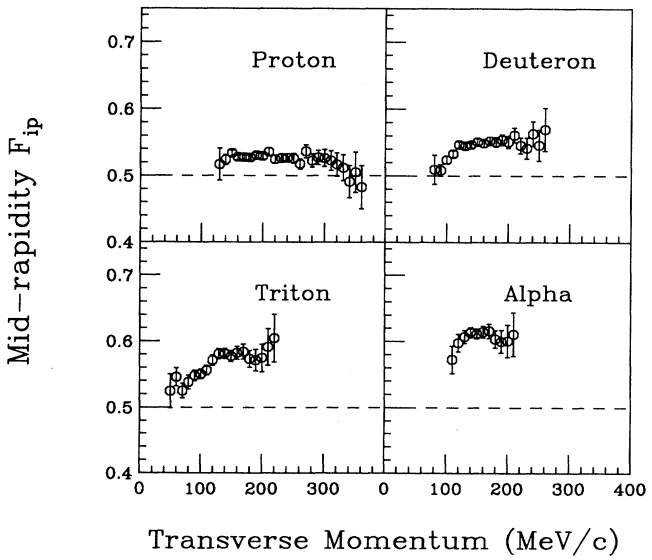

FIG. 10. Anisotropy fractions for 35 MeV/nucleon Ar+V data as function of $p^{\perp}$/nucleon. The rapidity of the particles was restricted to $y_{c.m.} \pm 0.02$ for this figure.

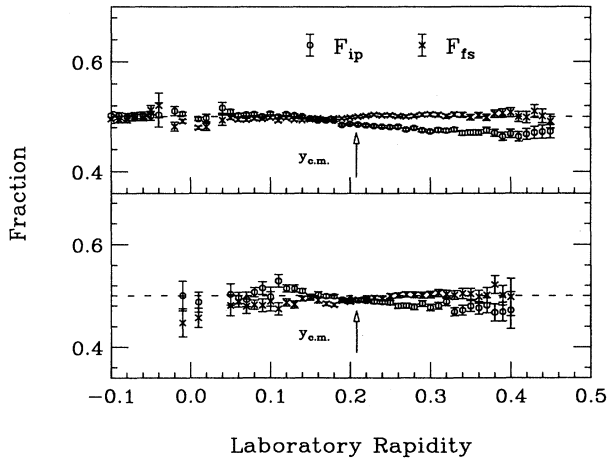

FIG. 12. Anisotropy fractions as function of rapidity for 100 MeV/nucleon Ar+V data.

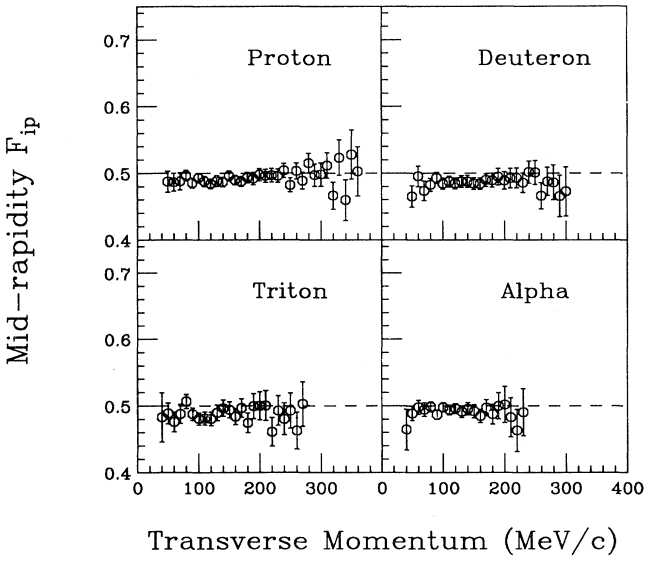

FIG. 13. Anisotropy fractions for 100 MeV/nucleon Ar+V data as function of $p^{\perp}$/nucleon. The rapidity of the particles was restricted to $y_{\text{c.m.}} \pm .02$ for this figure.

verse momentum in the reaction plane as a function of beam energy. The flow was found to exhibit a minimum at a beam energy between 80 and 90 MeV/nucleon for this system [15]. This observation has been interpreted as evidence for the balancing of the attractive and repulsive components of the nuclear mean field [7].

The general in-plane enhancement decreases monotonically with increasing beam energy. In Fig. 14, the maximum $F_{\text{ip}}(y)$ (i.e., taken from the region immediately below mid rapidity) is displayed as a function of the beam energy. Unlike flow, the collective motion creating the in-plane enhancement shows no minimum over this energy range. The increasing isotropy adds to the experimental evidence that fusion to form a compound system becomes more incomplete as the beam energy increases. (See Ref. [17] and references therein.)

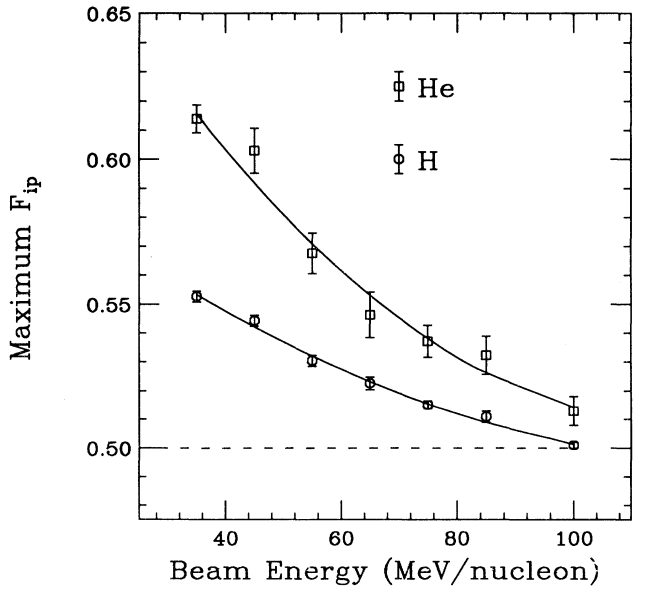

FIG. 14. The maximum of $F_{\text{ip}}(y)$ is used to measure the in-plane focusing of light particles produced in Ar+V collisions as a function of beam energy. The lines are drawn to guide the eye.

V. BUU CALCULATIONS

In order to know more about the two simple modes of collective motion under investigation and their influence on azimuthal distributions, we have performed an exploratory BUU calculation. (See Ref. [16] for a review of the BUU model.) The system used was a 30 MeV/nucleon mass-40 projectile incident on a symmetric target with a 2 fm impact parameter. This impact parameter is sufficiently central to guarantee the fusion of the projectile and target into a compound system. The effects of the Coulomb force were not included in the calculation. The interaction with the mean field was taken to be momentum independent, and was parametrized by a density-dependent Skyrme interaction with a compressibility of 380 MeV. Previous BUU studies [7,18] have demonstrated that collective motion near this beam energy is not very sensitive to the compressibility since there is insufficient energy to explore nuclear densities far from normal density. The magnitude of the in-medium nucleon-nucleon cross section was found to be more important; in our calculation we used $\frac{1}{2}$ of the free value. The energy and angular dependence of the nucleon-nucleon scattering was chosen to match free neutron-proton scattering [19]. For the n-n scattering calculations, the 30 000 test particles were divided into 375 parallel ensembles, and scattering was only allowed among nucleons within individual ensembles [16].

The detailed dependence of the collective motion on the n-n cross section, compressibility, and impact parameter should be explored in the future using codes which include the Coulomb force and the momentum dependence of the mean-field interaction. In addition, a thorough theoretical study on the contribution of the nuclear surface needs to be conducted before detailed comparisons can be made with experimental observations. The goal of our exploratory calculation was only to classify the modes of collective motion produced in a collision and characterize their influence on azimuthal distributions.

The decay of a rotating Ca nucleus with various initial excitation energies and angular momenta has been studied by Garcias *et al.* [20] using a similar microscopic transport equation. They found that a system could dissipate enough angular momentum through particle evaporation to avoid fission and multi fragmentation if the excitation energy was large enough relative to the angular momentum. They did not investigate the azimuthal distribution of the evaporated particles. In addition, since their initial state was a rigidly rotating sphere, their calculation did not attempt to explore the complex dynamics of an actual collision. In our calculation, we investi-

gated both of these issues.

First, we will examine the time development of the residue formed during the collision. In Fig. 15 we show snapshots of the coordinate space density projected onto the reaction plane. After a time of 30 fm/c, a deformed compound system is apparent which rotates about the y axis. In order to study this system, it is necessary to distinguish between particles which have been emitted and those which are still bound in the residue. This residue is visible in Fig. 16 which shows the number density of nucleons as a function of the distance from the c.m. after 150 fm/c. In order to isolate the residue, we assumed that all particles with space coordinates lying inside a region of local density greater than $\frac{1}{10}\rho_0$ were members of the residue. All other particles were taken as emitted particles. Since the residue is created by the nuclear mean field generated from the contributions of all of the separate ensembles in the calculation, the local density used to test for inclusion in the residue was the ensemble-averaged density.

For each quantity that follows, error bars were obtained by performing the calculation (for all the parallel ensembles) 4 times, finding the mean value of the quantity and then the uncertainty in the mean from the variances.

Following Garcias *et al.* [20], we use Hill-Wheeler [21] coordinates to study the changes in shape of the residue. The lengths of the semi major axes were parametrized using the square roots of the eigenvalues of the 3×3 matrix $\sum_{n=1}^{N} x_i^n x_j^n$ where N is the number of test particles in the residue. The result is shown in Fig. 17 with time intervals of 15 fm/c separating the small circles. There are strong oscillations from prolate to more oblatelike shapes, with the largest prolate deformation in the t=60 fm/c snapshot. If the beam energy had been higher or the impact parameter larger, the system could have proceeded to fission at this stage. Instead, the attractive mean field pulls the nucleons back toward the c.m., leading to a series of oscillations with decreasing amplitudes. Garcias *et al.* did not encounter these oscillations in their BUU calculations because they began with an equilibrated spherical system.

In Fig. 18 we show the change in the populations of

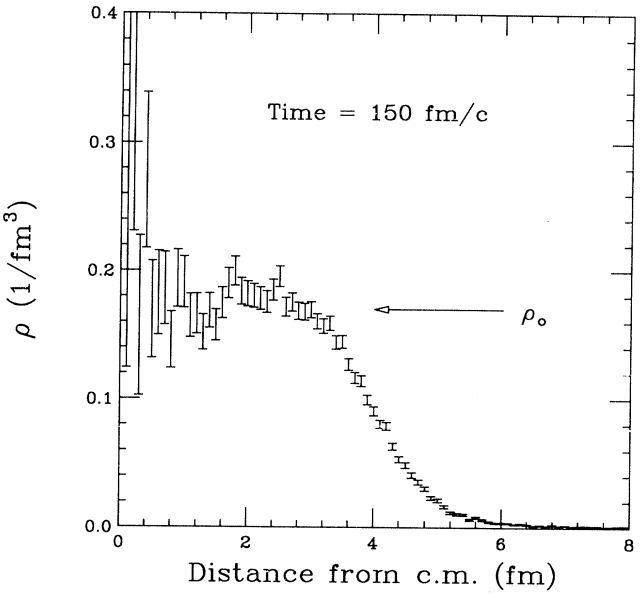

FIG. 16. Number density of nucleons as a function of distance from the center of mass in coordinate space at t=150 fm/c for one BUU calculation. The error bars in this figure are taken from the square root of the number of counts. Normal nuclear matter density is indicated by the arrow.

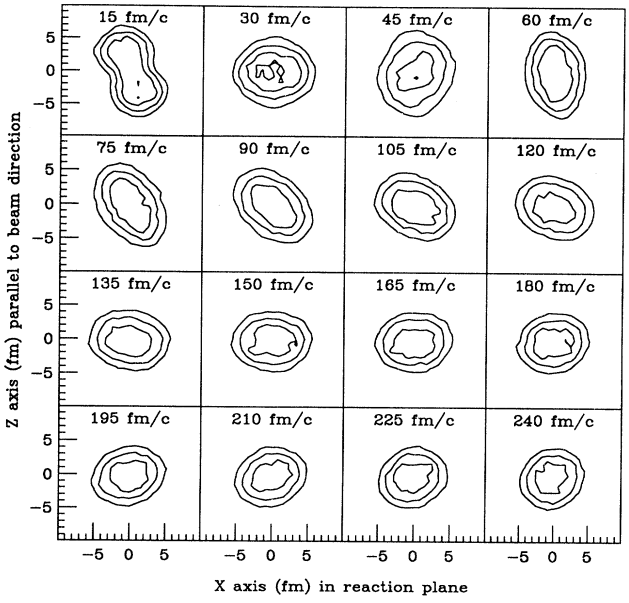

FIG. 15. BUU coordinate space density distribution projected on to the x-z plane. The projectile begins on the lower right-hand region in the 15 fm/c snapshot, offset in the positive x direction by convention.

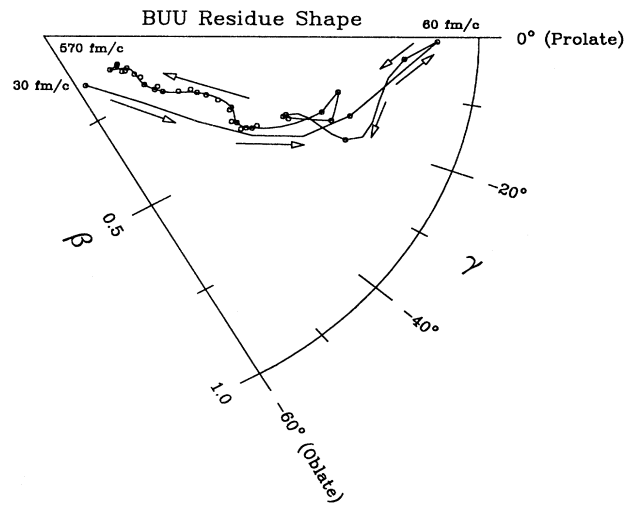

FIG. 17. Evolution of BUU residue in Hill-Wheeler coordinate space. The snapshots, denoted by small circles, are plotted from t=30 fm/c to t=570 fm/c in 15 fm/c intervals. The line and the arrows are drawn to guide the eye.

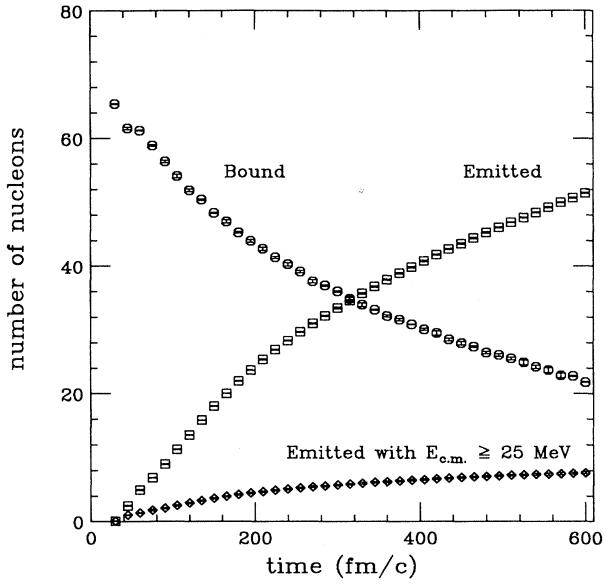

FIG. 18. The number of nucleons in the residue (circles) and the number of nucleons emitted (squares) are shown as a function of time for the BUU calculation. Those emitted with a center-of-momentum energy greater than 25 MeV are denoted by diamonds.

residue nucleons and emitted nucleons with time. The total number of nucleons is slightly less than $A_{\rm proj}+A_{\rm targ}$ because some nucleons can be less than 10 fm away from the center of mass, yet not be bound in the residue. Nucleons with c.m. kinetic energies in excess of 25 MeV come primarily from the earlier stages of the reaction. For reference, the energy of the projectile and target in the center of mass is ≈ 7.5 MeV/nucleon. It is the addition of the intrinsic Fermi energy and the beam energy that allows the production of these high-energy nucleons.

Next we turn to a consideration of the angular momentum. The angular momentum of the residue is denoted by circles in Fig. 19. Beginning with $\approx 40\hbar$ the residue loses angular momentum at a decreasing rate with time. All the angular momentum lost by the residue is accounted for in the emitted particles (denoted by squares), indicating that the calculation conserves angular momentum in a collision on average. At the end of the calculation, almost all of the angular momentum of the residue has been carried away.

If we examine the final distribution of nucleons emitted from the simulated collisions, we find both of the patterns of collective motion that we observed in the data earlier. In Fig. 20 the anisotropy parameters extracted from the BUU calculation after 570 fm/c are denoted by circles. The fractions were generated using the known reaction plane of the simulation, and calculated as a function of an artificially imposed c.m. energy threshold. In order to improve the statistics, $F_{\rm ip}(y)$ was calculated from azimuthal distributions summed over all rapidities. The fraction of particles in the reaction plane increases with the energy threshold, as expected for rotational collective motion.

The new flow parameter is $\Delta F_{\rm fs}(y)$, the difference between the $F_{\rm fs}(y)$ of particles going forward and those going backward in the c.m. frame of reference. The choice of the forward flow side was made such that a repulsive side splash would result in a positive $\Delta F_{\rm fs}(y)$ parameter. The negative value of $\Delta F_{\rm fs}(y)$ is due to the attractive deflection experienced by the nucleons during their interaction via the mean field.

The two types of anisotropies result from collective motions that occur at different times during the calculation. We demonstrate this in Fig. 20 by plotting as crosses the anisotropy parameters for particles emitted only after the first 60 fm/c of the collision. This removes the contribution from "promptly emitted particles" (PEP's),

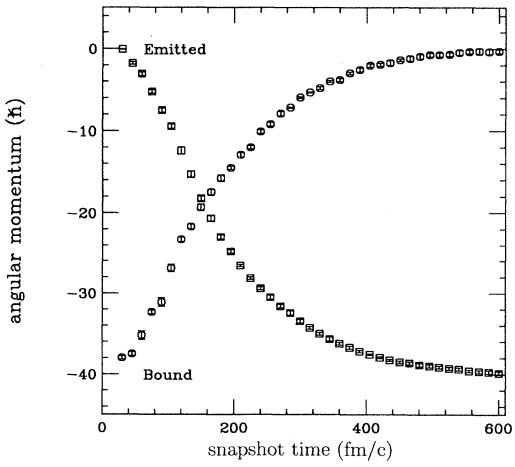

FIG. 19. Angular momentum in the BUU calculation as a function of time.

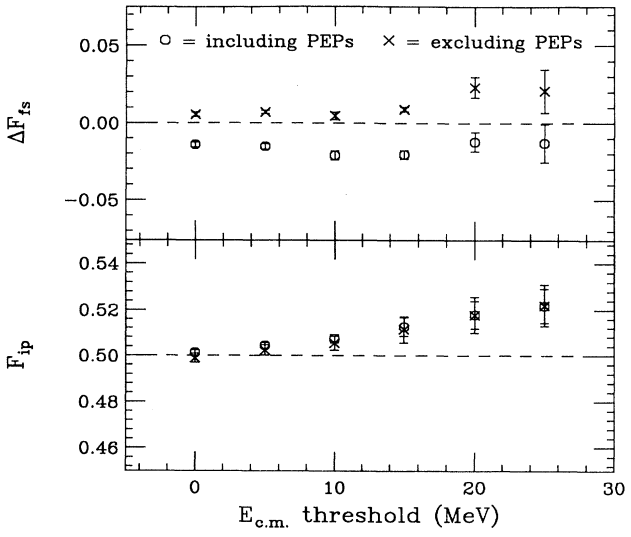

FIG. 20. Final BUU anisotropy fractions calculated with and without including nucleons emitted in the first 60 fm/c (PEP's).

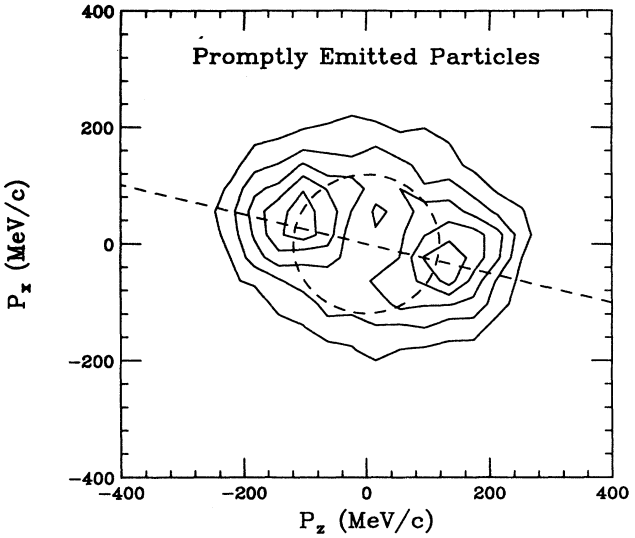

FIG. 21. Momentum distribution of particles emitted in the first 60 fm/c of the BUU calculation projected onto the reaction plane in the c.m. frame of reference.

in this case approximately the first five emitted nucleons. The flow parameter $\Delta F_{\rm fs}(y)$ shows no negative flow at all when PEP's are excluded. The flow in this BUU calculation is thus due to the very first particles emitted in the collisions. On the other hand, removing the PEP's from the sample has practically no effect on the in-plane enhancement, indicating that this anisotropy is formed over a longer time period as the decaying system dissipates angular momentum through particle emission.

The strong mean field deflection of PEP's can be easily seen in Fig. 21, which displays the projection onto the reaction plane of the momentum distribution of particles emitted in the first 60 fm/c after contact. Contact is taken as the moment when the centers of the projectile and target are separated by a distance equal to the sum of their radii. The dashed circle has a radius of 120 MeV/c, approximately the c.m. momentum of the nucleons neglecting the Fermi momentum. The dashed line is at the angle with respect to the beam axis made by the centers of the two nuclei when they first contact. There is enhanced emission of particles with the c.m. beam velocity deflected by the angle joining the centers of the two nuclei at their first contact.

Because of Pauli blocking of collisions, some nucleons of the projectile can pass directly through the target. The addition of the intrinsic Fermi motion to the projectile motion allows particles to directly escape the mean field of the target and vice versa. Early models of promptly emitted particles based on simple geometrical concepts predicted that such "Fermi jets" will be aligned with the axis joining the center of the projectile and target when they first contact [22–24]. The simple geometry and assumptions used in the Fermi jet picture have been replaced by more detailed dynamical calculations which include absorption and scattering of potential jets [25]. A full microscopic model like BUU that contains Fermi momentum, the mean field, n-n scattering, and Pauli blocking automatically contains all of these prompt emission processes. Thus, it is not surprising that the first particles emitted in the calculation show the effect of mean field deflection more clearly than particles emitted later whose motions have been randomized by successive n-n collisions.

VI. CONCLUSIONS

From our observations of the azimuthal distributions of light particles produced in intermediate-energy heavy-ion collisions, we can conclude that there is sufficient collective motion to cause substantial azimuthal anisotropies with respect to the reaction plane. We have confirmed the work of others who first noted enhanced emission in the reaction plane [1], and extended their work to lighter, more symmetric systems and to higher beam energies. In addition, we have identified a separate azimuthal anisotropy due to collective flow and developed a parametrization which distinguishes between the two modes of collective motion. Both anisotropies increase with the mass of the particle of interest, as would be expected if a collective velocity was superimposed on random thermal motion.

Both forms of collective motion change in character as the beam energy is increased, with flow showing a minimum between 80 and 90 MeV/nucleon [15] and rotation decreasing in importance as the beam energy goes to 100 MeV/nucleon. The minimum in the collective flow between 80 and 90 MeV/nucleon is consistent with BUU predictions that the hard core repulsive part of the mean field should create a hydrodynamical side splash which cancels the attractive mean field deflection near this beam energy [7]. As for the general in-plane enhancement, increasing the beam energy may simply overcome the ability of the mean field to form a compound rotating system.

Both forms of anisotropy are consistent with the influence of an attractive mean field. Our initial explorations using BUU calculations show that the in-plane enhancement is established as the compound system created by the mean field dissipates its angular momentum through particle emission. The azimuthal anisotropy due to flow is due to the attractive mean field deflection of promptly emitted particles. The calculation confirms that both forms of collective motion can be present in one collision, although they reflect the dynamics of the reaction at different times.

ACKNOWLEDGMENTS

We would like to thank S. Howden and J. Karn for their help during the data acquisition. We would also like to thank Professor W. Benenson, Professor P. Danielewicz, and B. Young for their help during the data analysis. This work was supported in part by the National Science Foundation under Grant No. PHY-89-13816.

APPENDIX

In addition to the anisotropy fractions presented in this paper, two other parametrizations have been used to characterize the azimuthal distributions produced in heavy-ion collisions. In this appendix we will derive the relationships between our parametrization and those employed by other authors.

Peak/valley ratios or in/out of plane ratios are used to characterize the in-plane enhancement observed in heavy-ion collisions [1,26]. The ratio R is defined by

$$R = \frac{\left.\frac{dN}{d\phi}\right|_{\phi=0^\circ}}{\left.\frac{dN}{d\phi}\right|_{\phi=90^\circ}}, \tag{A1}$$

where ϕ is the azimuthal angle around the beam axis with respect to the reaction plane and N is the number of particles detected. The connection with the $F_{\rm ip}(y)$ parameter is

$$R = \frac{1+\pi[F_{\rm ip}(y)-\frac{1}{2}]}{1-\pi[F_{\rm ip}(y)-\frac{1}{2}]} \tag{A2}$$

and

$$F_{\rm ip}(y) = \frac{1}{2} + \frac{R-1}{\pi(R+1)} \tag{A3}$$

if the azimuthal distribution is of the form

$$\frac{dN(\phi)}{d\phi} \propto 1 + a\cos(2\phi). \tag{A4}$$

We chose not to use this parametrization because it is inappropriate for describing flow. Even if the ratio is taken between $\phi = 0^\circ$ and $\phi = 180^\circ$, there are still problems with the symmetry of the deviation from isotropy as a function of rapidity. This can be illustrated by a simple example. Consider a case in which twice as many particles appear on the forward flow side as compared to the opposite side of the reaction plane at high rapidities. Then, for a symmetric system, at low rapidities the forward flow side would contain half as many particles as its opposite. Our $F_{\rm fs}(y)$ parameter would go from $\frac{1}{3}$ to $\frac{2}{3}$, passing through $\frac{1}{2}$ at mid rapidity. The deviation from isotropy would go from -0.17 to $+0.17$, making a symmetric curve like that shown in Fig. 4. Now consider the behavior of R taken between opposite sides of the reaction plane. At high rapidities $R = 2$, while at low rapidities $R = \frac{1}{2}$. Isotropy is represented by a ratio of 1, and so the deviation from isotropy goes from $-\frac{1}{2}$ to 1, and is asymmetric around mid rapidity. The effect is to exaggerate the flow in the forward c.m. direction at the expense of the flow in the backward direction.

For a particular value of the parallel rapidity, flow causes particles to be deflected preferentially to one side of the reaction plane. This behavior can be included into Eq. (A4) by the addition of another term:

$$\frac{dN(\phi,y)}{d\phi} \propto 1 + a(y)\cos(2\phi) + b(y)\cos(\phi). \tag{A5}$$

In eq. A5 the parameter $a(y)$ is sensitive to the enhancement that occurs simultaneously on both sides of the reaction plane (rotation), while $b(y)$ is sensitive to flow. This parametrization has been employed by the Plastic Ball Group [27] and others [28]. Integrating Eq. (A5) over the appropriate ϕ regions, we find that our anisotropy parameters are given by

$$F_{\rm ip}(y) = \frac{1}{2} + \frac{a}{\pi} \tag{A6}$$

and

$$F_{\rm fs}(y) = \frac{1}{2} + \frac{b}{\pi}. \tag{A7}$$

These results also demonstrate that $F_{\rm ip}(y)$ is only sensitive to rotation and $F_{\rm fs}(y)$ is only sensitive to flow within this parametrization.

[1] M.B. Tsang, C.B. Chitwood, D.J. Fields, C.K. Gelbke, D.R. Klesch, W.G. Lynch, K. Kwiatkowski, and V.E. Viola, Jr., Phys. Rev. Lett. **52B**, 1967 (1984).

[2] W.K. Wilson, W. Benenson, D.A. Cebra, J. Clayton, S. Howden, J. Karn, T. Li, C.A. Ogilvie, A. Vander Molen, G.D. Westfall, J.S. Winfield, B. Young, and A. Nadasen, Phys. Rev. C **41**, R1881 (1990).

[3] H. Stöcker, J.A. Maruhn, and W. Greiner, Phys. Rev. Lett. **44**, 725 (1980).

[4] P. Danielewicz and G. Odyniec, Phys. Lett. **157B**, 146 (1985).

[5] H.H. Gutbrod, A.M. Poskanzer, and H.G. Ritter, Rep. Prog. Phys. **52**, 1267 (1989).

[6] M.B. Tsang, R.M. Ronningen, G. Bertsch, Z. Chen, C.B. Chitwood, D.J. Fields, C.K. Gelbke, W.G. Lynch, T. Nayak, J. Pochodzalla, T. Shea, and W. Trautmann, Phys. Rev. Lett. **57**, 559 (1986).

[7] C.A. Ogilvie, W. Bauer, D.A. Cebra, J. Clayton, S. Howden, J. Karn, A. Nadasen, A. Vander Molen, G.D. Westfall, W.K. Wilson, and J.S. Winfield, Phys. Rev. C **42**, R10 (1990).

[8] W.K. Wilson, D. Cebra, S. Howden, J. Karn, D. Krofcheck, R. Lacey, T. Li, A. Nadasen, T. Reposeur, A. Vander Molen, C.A. Ogilvie, G.D. Westfall, and J.S. Winfield, Phys. Rev. C **43**, 2696 (1991).

[9] G.D. Westfall, J.E. Yurkon, J. Van der Plicht, Z.M. Koenig, B.V. Jacak, R. Fox, G.M. Crawley, M.R. Maier, and B.E. Hasselquist, Nucl. Instrum. Methods A **238**, 347 (1985).

[10] C.A. Ogilvie, D.A. Cebra, J. Clayton, P. Danielewicz, S. Howden, J. Karn, A. Nadasen, A. Vander Molen, G.D. Westfall, W.K. Wilson, and J.S. Winfield, Phys. Rev. C **40**, 2592 (1989).

[11] C.A. Ogilvie, D.A. Cebra, J. Clayton, S. Howden, J. Karn, A. Vander Molen, G.D. Westfall, W.K. Wilson, and J.S. Winfield, Phys. Rev. C **40**, 654 (1989).

[12] W.K. Wilson, R. Lacey, C.A. Ogilvie, and G.D. Westfall, Phys. Rev. C **45**, 738 (1992).

[13] M.B. Tsang, W.G. Lynch, C.B. Chitwood, D.J. Fields, D.R. Klesch, C.K. Gelbke, G.R. Young, T.C. Awes, R.L.

Ferguson, F.E. Obenshain, F. Plasil, and R.L. Robinson, Phys. Lett. **148B**, 265 (1984).
[14] C.B. Chitwood, D.J. Fields, C.K. Gelbke, D.R. Klesch, W.G. Lynch, M.B. Tsang, T.C. Awes, R.L. Ferguson, F.E. Obenshain, F. Plasil, R.L. Robinson, and G.R. Young, Phys. Rev. C **34**, 858 (1986).
[15] D. Krofcheck, D.A. Cebra, M. Cronqvist, R. Lacey, T. Li, C.A. Ogilvie, A. Vander Molen, K. Tyson, G.D. Westfall, W.K. Wilson, J.S. Winfield, A. Nadasen, and E. Norbeck, Phys. Rev. C **43**, 350 (1991).
[16] G.F. Bertsch and S. Das Gupta, Phys. Rep. **160**, 190 (1988).
[17] K. Hagel, A. Péghaire, G.M. Jin, D. Cussol, H. Doubre, J. Péter, F. Saint-Laurent, G. Bizard, R. Brou, M. Louvel, J.P. Patry, R. Regimbart, J.C. Steckmeyer, B. Tamain, Y. Cassagnou, R. Legrain, C. Lebrun, E. Rosato, R. Macgrath, S.C. Jeong, S.M. Lee, Y. Nagashima, T. Nakagawa, M. Ogihara, J. Kasagi, and T. Motobayashi, Phys. Lett. **B229**, 20 (1989).
[18] G.F. Bertsch, W.G. Lynch, and M.B. Tsang, Phys. Lett. **B189**, 384 (1987).
[19] Particle Data Group, Phys. Lett **B204**, 126 (1988).
[20] F. Garcias, V. De La Mota, B. Remaud, G. Royer, and F. Sébille, Phys. Lett. **B265**, 311 (1991).
[21] D.L. Hill and J.A. Wheeler, Phys. Rev. **89**, 1102 (1953).
[22] M.C. Robel, Lawerence Berkeley Laboratory Report No. LBL-8181, 1979.
[23] J.P. Bondorf, J.N. De, A.O.T. Karvinen, G. Fái, and B. Jakobsson, Phys. Lett. **84B**, 162 (1979).
[24] J.P. Bondorf, J.N. De, A.O.T. Karvinen, G. Fái, B. Jakobsson, and J. Randrup, Nucl. Phys. **A333**, 285 (1980).
[25] J. Randrup and R. Vandenbosch, Nucl. Phys. **A474**, 219 (1987).
[26] M.B. Tsang, Y.D. Kim, N. Carlin, Z. Chen, C.K. Gelbke, W.G. Gong, W.G. Lynch, T. Murakami, T. Nayak, R.M. Ronningen, H.M. Xu, F. Zhu, L.G. Sobotka, D.W. Stracener, D.G. Sarantities, Z. Majka, and V. Avenante, Phys. Rev. C **42**, R15 (1990).
[27] H.H. Gutbrod, K.H. Kampert, B. Kolb, A.M. Poskanzer, H.G. Ritter, R. Schicker, and H.R. Schmidt, Phys. Rev. C **42**, 640 (1990).
[28] G.M. Welke, M. Prakash, T.T.S. Kuo, S. Das Gupta, and C. Gale, Phys. Rev. C **38**, 2101 (1988).